



# Analytical modeling and multi-objective optimization algorithm for abrasive waterjet milling Ti6Al4V

Liang Wan<sup>1,2</sup> · Jiayang Liu<sup>2</sup> · Yi'nan Qian<sup>1,2</sup> · Xiaosun Wang<sup>1,2</sup> · Shijing Wu<sup>1,2</sup> · Hang Du<sup>2</sup> · Deng Li<sup>1,2</sup> 

Received: 28 June 2022 / Accepted: 30 October 2022 / Published online: 19 November 2022  
© The Author(s), under exclusive licence to Springer-Verlag London Ltd., part of Springer Nature 2022

## Abstract

Abrasive waterjet (AWJ) is a promising method for machining titanium alloy, which is widely used in the aerospace field, but the various process parameters of AWJ make it difficult to achieve a high machining quality. In this research, the main process parameters of AWJ, including the jet pressure, the abrasive flow rate, the stand-off distance, the jet angle, the traverse speed, and the feed rate, were all analyzed by considering their effects on the milling characteristics of Ti6Al4V alloy. Both single and interactive effects of the process parameters were studied, and regression models for predicting the milling depth  $h$ , the material erosion rate  $\dot{V}$ , and the X-directional roughness  $Ra_x$  were established. Furthermore, an ADM-MO-Jaya (adaptive decreasing method multi-objective Jaya) algorithm based on MO-Jaya was proposed to obtain the optimal process parameters, aiming for reaching the minimum  $Ra_x$  and the maximum  $h$  and  $\dot{V}$  at the same time. The results show that the correlation coefficients  $R^2$  of the models are all greater than 0.9, and model terms are relatively significant. The regression models of  $h$ ,  $\dot{V}$ , and  $Ra_x$  are generally consistent with the overall trend of the experimental results, and the mean errors are 8.57%, 1.89%, and 10.58%, respectively. The operation efficiency of the ADM-MO-Jaya algorithm is 32% higher than that of the MO-Jaya, and the Pareto front is the most uniform and converges to a curve in the solution space without isolated points. The optimized set of 180 Pareto solutions can be directly selected by the operator for machining without complex process comparisons, which can guide the practical milling of titanium alloy by AWJ.

**Keywords** Titanium alloy · Abrasive waterjet milling · Process parameters · Regression analysis · Multi-objective optimization

## 1 Introduction

Due to its high specific strength, high-temperature resistance, corrosion resistance, and high biocompatibility, titanium alloy is being widely used in aerospace, petrochemical, and biomedical fields. However, its poor thermal conductivity and strong chemical activity in high-temperature environments make it very difficult to process [1]. Currently, some scholars study the machining and laser processing of titanium alloys [2]. It was found that the tool is easy to wear due to its high material removal rate [3]. The huge heat generated by machining and laser processing can easily burn the

parts, which has a great impact on the service life of titanium alloy parts [4].

AWJ machining technology has received a lot of attention by virtue of its environmental friendliness, high material removal rate, and no cutting heat to burn parts. In recent decades, more and more research has focused on the cutting of titanium alloys by AWJ. A numerical model based on smooth particle dynamics was developed to simulate the cutting of titanium alloys by AWJ, showing that the shape of the abrasive grain played an important role in the cutting efficiency and the cutting trajectory. Similarly, the sharpness of the abrasive also strongly affected the material removal rate [5]. To shed light on the influence of pressure, traverse speed, stand-off distance, and other parameters on cutting efficiency and surface quality, a large number of AWJ cutting experiments were carried out [6–8]. According to the results, the roughness of the cutting surface can be reduced by higher pressure, a larger abrasive flow rate, a lower traverse speed, and a smaller abrasive grain. The cutting taper

✉ Deng Li  
2008lee@whu.edu.cn

<sup>1</sup> Hubei Key Laboratory of Waterjet Theory and New Technology, Wuhan University, Wuhan 430072, China

<sup>2</sup> School of Power and Mechanical Engineering, Wuhan University, Wuhan 430072, China

will decrease under the condition of higher pressure and a larger abrasive grain, while it will increase with a higher transverse speed. The material erosion rate will increase with a higher abrasive flow rate. Considering the effects of abrasive grain, abrasive flow rate, and the number of cuts on the cutting depth, an orthogonal experiment of AWJ cutting titanium alloy was designed [9, 10]. The results showed that a larger abrasive grain and abrasive flow rate could improve the cutting depth and reduce the cutting cone angle. Compared with a single cutting, the multiple-cutting performance was significantly improved. Fuse et al. [11] designed cutting experiments on titanium alloy by AWJ based on the response surface method and analyzed the effects of traverse speed, abrasive flow rate, and stand-off distance on material removal rate, surface roughness, and taper. Furthermore, ANOVA was performed to further verify the robustness of the system.

The milling of titanium alloys by AWJ has also been studied by some scholars. It is considered that the process of material milling can be viewed as the superposition of multiple single milling section profiles along the feed direction. Therefore, the maximum depth and width of the footprints of single milling and the amount of overlap in the feed direction can have a significant effect on the material removal rate and the surface roughness [12–14]. The effects of different types of abrasives on milling titanium alloys were investigated, and the results showed that the hardness of the workpiece and the hardness of the abrasive had a greater impact than the shape of the abrasive. When the hardness of the abrasive increased, both the material removal rate and the surface roughness increased [15]. The footprints of single milling and multiple overlapping milling of AWJ were simulated by the finite element method and the Johnson–Cook failure criterion, respectively. Compared with the experimental data, the maximum depth error of simulation models for single milling and multiple overlapping milling were within 10 and 15%, respectively [13, 16]. A milling method based on iterative learning control was proposed. The results showed that the milling depth error was reduced by more than 50% after 4 iterations [17]. An empirical formula for the depth of titanium alloy milling by AWJ was established based on the conservation of energy and momentum, and the validation data showed that the average error of the model was within 15% [18].

At present, nontraditional optimization algorithms have been introduced to optimize the abrasive machining process. For example, an artificial bee colony algorithm was used to optimize the process of cutting aluminum alloy by AWJ, resulting in a lower surface roughness value compared to the neural network algorithm, genetic algorithm, and simulated annealing method [19]. The cuckoo algorithm was applied to optimize the surface roughness of aluminum alloy cutting by AWJ, which could effectively improve the surface

roughness to that of artificial neural networks and support vector machines [20]. Although the researchers have made great achievements in terms of depth, roughness, and material erosion rate after processing by AWJ with a single objective optimization algorithm. AWJ machining is a typical multiple-input, multiple-output process, and a simple single-objective optimization cannot simultaneously be taken into account the roughness and machining efficiency. In the past, the selection of the best parameters relied mainly on the rich machining experience of the workers, which not only relied too much on the operator but also made it very difficult for process planning. Therefore, it is particularly important to obtain as high machining efficiency as possible to reduce production costs while maintaining surface roughness.

On the other hand, multi-objective optimization of material removal rate and surface roughness for cutting by AWJ was carried out by the Gray Wolf algorithm. The results showed that the algorithm converged faster and achieved better results [21]. Optimization algorithms such as particle swarm, firefly, and simulated annealing were used to study the effects of traverse velocity, stand-off distance, and abrasive flow rate on the top width and taper angle after cutting by AWJ. A set of non-dominated solutions were successfully found and verified by experiments [22]. Based on the response surface analysis and heat transfer search algorithm, the taper angle, material removal rate, and surface roughness of titanium alloy after cutting by AWJ were optimized. As a result, the difficulty and complexity of machining be greatly reduced according to a set of Pareto optimal solutions obtained [11]. Recently, Rao et al. proposed a new minimalist optimization algorithm Jaya, different from the existing evolutionary algorithms, it has a simple structure and is easy to implement programmatically without too many tuning parameters to deal with, avoiding the risk of falling into a local optimum due to improper adjustment of specific parameters of the algorithm by the user. Good optimization results were obtained when it was used for multi-objective optimization of taper angle and surface roughness after cutting by AWJ [23–25].

Therefore, it can be found that the studies on the parameters of AWJ milling titanium alloys are much fewer compared to that of cutting titanium alloys. In addition, the milling parameters that have been considered in the earlier research studies are not complete enough. In our study, the process parameters such as jet pressure, abrasive flow rate, stand-off distance, jet angle, traverse speed, and feed rate are fully considered, which will not only lead to the higher prediction accuracy of the milling model but also increase the flexibility of AWJ machining to some extent. Thus, we designed an experiment for milling titanium alloy by AWJ. The relationship between the effect of AWJ machining parameters on milling depth, material erosion rate, and surface roughness was analyzed based on the response surface

method. We established regression models for milling depth, material erosion rate, and surface roughness and further assessed the robustness of the models by ANOVA. For any processing method, processing efficiency is an extremely important economic indicator. High processing efficiency not only saves time for the factory but also reduces the consumption of energy. Material erosion rates are widely used in abrasive jet machining to measuring process efficiency. Considering that the existing studies on the milling of titanium alloys by AWJ are often limited to single-objective optimization and bi-objective optimization for milling depth and surface roughness, no one has yet performed multi-objective optimization for milling depth, material removal rate, and surface roughness. Therefore, the tri-objective optimization algorithm ADM-MO-Jaya optimization algorithm for surface roughness, milling depth, and material erosion rate of titanium alloy milled by abrasive jet is applied for the first time to obtain the maximum milling depth and material erosion rate while ensuring surface roughness. At the same time, the algorithm is improved to obtain not only a uniformly distributed Pareto front but also to reduce the time consumed for convergence, which is of great significance for AWJ milling of titanium alloys.

The remainder of this paper is organized as follows: Section 2 describes the experiment of milling titanium alloy by AWJ. Section 3 presents the principle of the proposed method and introduces the improvement of the multi-objective optimization algorithm. Section 4 is mainly for the analysis and discussion of the experimental results. Finally, conclusions are presented in Section 5.

## 2 The experiment of milling titanium alloy by AWJ

### 2.1 Experimental equipment and materials

Experiments were carried out on the ultra-high-pressure AWJ five-axis machining platform (APW-P410-L6-N200) at Hubei Key Laboratory of Waterjet Theory and New Technology (Fig. 1) with a maximum working pressure of 420 MPa and a jet angle adjustment around X-axis range of  $-90^\circ$  to  $90^\circ$ . The equipment adopts a post-mixing priming method for sand supply, and the abrasive flow rate can be regulated from 100 to 760 g/min. The nozzle material is ruby with an inner diameter of 0.33 mm. The inner diameter of the focusing tube was 1.02 mm, and the length was 76.2 mm. The abrasive used in the experiments was 80-mesh garnet. The specimen was a Ti6Al4V alloy plate with excellent comprehensive mechanical properties, and its main physical and chemical compositions are shown in Table 1.

### 2.2 Milling path and evaluation factor

Due to the influence of the jet stagnation effect, concentric surround and helical milling are prone to overcutting, resulting in poor quality. The zig-zag milling path was selected, as shown in Fig. 2. It can be seen that there are obvious peaks and valleys between two adjacent milling paths along the feed direction (X-direction) from Fig. 3, so the roughness in this direction will be larger compared to the Y-direction. Usually, a larger roughness is chosen to measure the quality

**Fig. 1** Ultra-high pressure AWJ 5-axis CNC machining system

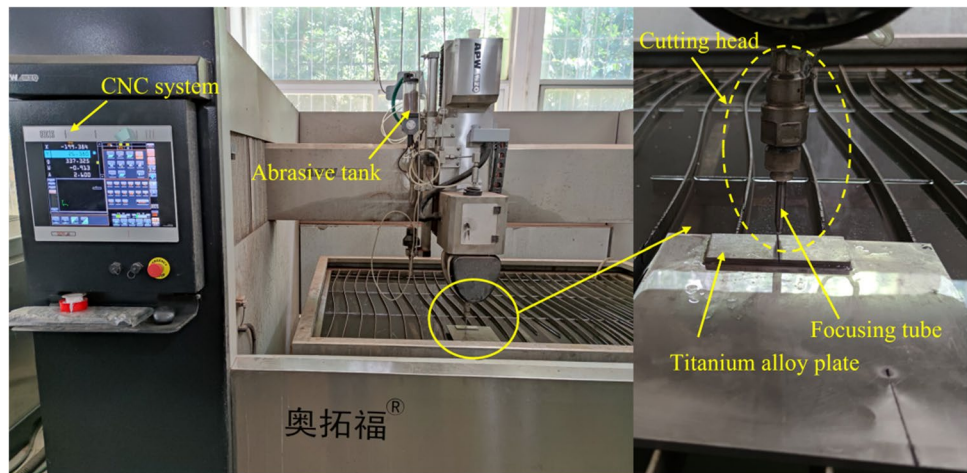


**Table 1** Main physical and chemical parameters of TC4 titanium alloy

| Material                          | $\sigma_s$ /(MPa) | $\sigma_b$ /(MPa) | $\rho$ /(g·cm <sup>3</sup> ) | Chemical composition (wt%)  |
|-----------------------------------|-------------------|-------------------|------------------------------|---|
| Ti <sub>6</sub> Al <sub>4</sub> V | ≥ 860             | ≥ 895             | 4.51                         | Al (5.5–6.8), V (3.5–4.5), Fe (≤0.3), C (≤0.1), O (≤0.2), N (≤0.05), H (≤0.015), Ti (residuals) |

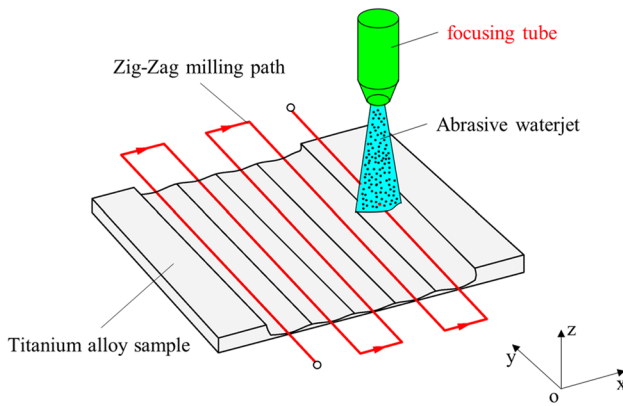


**Fig. 2** Abrasive waterjet milling path

of the machining. Therefore, the milling depth  $h$ , material erosion rate  $\dot{V}$ , and  $X$ -directional roughness  $Ra_x$  were selected as metrics to measure AWJ milling performance.  $h$  and  $Ra_x$  were measured with a ZYGO 3D optical profiler manufactured by AMETEK. The profiler has a scanning range of 0 to 20 mm, a scanning speed of more than 114  $\mu\text{m/s}$ , a surface roughness measurement accuracy of higher than 0.1 nm, a surface topography repetition accuracy of 0.01 nm, and a CCD camera resolution is  $1024 \times 1024$ .  $\dot{V}$  was obtained by dividing the mass difference before and after processing by density and time. Of course, it is necessary to dry the workpiece when measuring the mass.

The scanning results of the optical profilometer are shown in Fig. 3. The milling plane by AWJ was formed by the superposition of multiple single passes along the transverse direction. Influences such as secondary erosion of the reflective jet, residual stresses from the previous process, and the slope of the eroded surface need to be taken into account. Under the condition that the jet pressure  $P$ , abrasive flow rate  $\dot{m}_a$ , stand-off distance  $D$ , jet angle  $\alpha$ , and traverse speed  $u$  are determined, the feed rate  $S$  is an important process parameter affecting the milling profile. Too large an  $S$  will

produce a waveform plane, and too small an  $S$  will lead to the degradation of the bottom surface features. According to the experiments, Bui et al. [26] concluded that the preferred range of  $S$  is  $0.7b_{\max} \leq S \leq b_{\max}$ . The level of  $S$  was designed concerning the above-preferred range and pre-experiment in this research.

### 3 Analysis method and multi-objective optimization algorithm

#### 3.1 Response surface method and nonlinear regression

The response surface method based on Box–Behnken does not require the study of all process parameter combinations, significantly reducing the operation cost of the experiment and accurately estimating coefficients below the fifth order. According to the research of Hlavac et al. [27], the reliability of the statistical-regression model is high within the tested scope of factors. However, its precision can be significantly reduced beyond the selected range of factors. Considering that the main purpose of this paper is to investigate the effect of abrasive jet milling on titanium alloys and to obtain the optimal machining parameters. Therefore, the actual working conditions of abrasive jet milling of titanium alloys were considered. Based on extensive pre-experiments, the levels of each factor were reasonably designed to ensure that the range of common machining parameters was included in the setting of the levels. Table 2 shows the arrangement of each factor and level. The experimental protocol was carried out in Design-Expert software. Table 3 shows the specific arrangement and the results of the statistics.

The empirical models for  $h$ , and  $Ra_x$  can be obtained by nonlinear regression analysis of the experimental results in Table 3. Preliminary analysis shows that better models can be obtained by fitting the experimental data with a third-order model. Thus, taking the third order as an example,

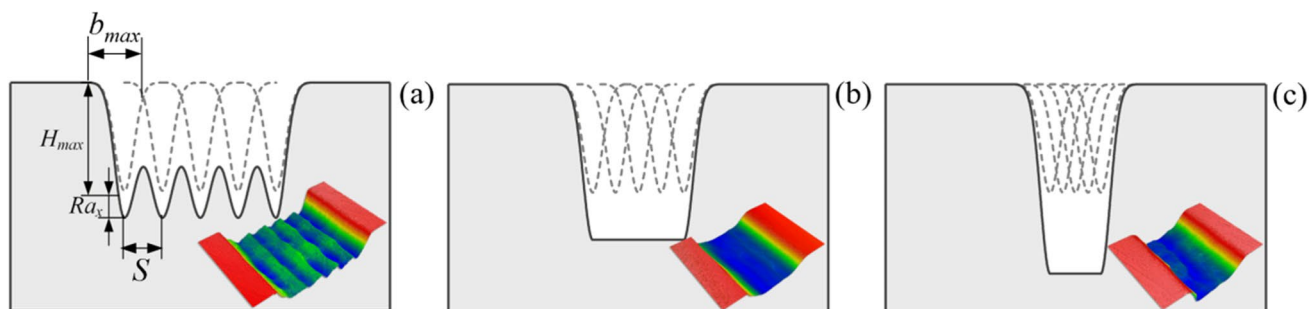


**Fig. 3** Effect of lateral feed on milling results; **a** too large  $S$ , **b** appropriate  $S$ , and **c** too small  $S$

**Table 2** Factors and levels of experimentation

| Process factors             | Level 1 | Level 2 | Level 3 |
|-----------------------------|---------|---------|---------|
|                             | − 1     | 0       | 1       |
| Jet pressure $P$ (MPa)      | 220     | 260     | 300     |
| Mass flow rate $a$ (g/min)  | 200     | 480     | 760     |
| Stand-off distance $D$ (mm) | 6       | 14      | 22      |
| Jet angle $\alpha$ (°)      | 30      | 60      | 90      |
| Traverse speed $u$ (mm/s)   | 30      | 50      | 70      |
| Feed rate $S$ (mm)          | 0.4     | 0.6     | 0.8     |

the general format of higher-order nonlinear regression is as follows:

$$\begin{aligned}
 Y = & \beta_0 + \sum_{i=1}^m \beta_i X_i + \sum_{i=1}^{m-1} \sum_{j=i+1}^m \beta_{ij} X_i X_j + \sum_{i=1}^m \beta_{ii} X_i^2 + \sum_{i=1}^{m-2} \sum_{j=i+1}^{m-1} \sum_{k=j+1}^m \beta_{ijk} X_i X_j X_k \\
 & + \sum_{i=1}^{m-1} \sum_{j=i+1}^m \beta_{ij} X_i X_j^2 + \sum_{i=1}^{m-1} \sum_{j=i+1}^m \beta_{ij} X_i^2 X_j + \sum_{i=1}^m \beta_{ii} X_i^3
 \end{aligned}
 \tag{1}$$

where  $Y$  is the response variable,  $X$  is each process parameter,  $\beta_0$  is the constant term, and  $\beta_i$ ,  $\beta_{ii}$ ,  $\beta_{ij}$ , and  $\beta_{ijk}$  are the coefficients of different order terms, respectively. ANOVA and residual diagnostics were used to test the reliability, significance, and accuracy of the models. It is worth noting that the parameter values of the model need to be converted into the level between − 1 and 1 according to Table 2.

### 3.2 Multi-objective optimization algorithm

The MO-Jaya algorithm is a multi-objective optimization algorithm that expands on the Jaya algorithm. To deal with the problem of the coexistence of multiple objectives, the MO-Jaya algorithm is embedded with a fast non-dominated sorting approach and crowding distance evaluation approach [25, 28]. The solution is chosen based on the non-dominated rank and the crowding distance  $\xi$ . For instance, the solution with the highest non-dominated rank (rank = 1) and the largest crowding distance  $\xi$  is selected as the best solution. Those solutions that are the opposite are chosen as the worst solutions. The best and worst solutions are selected and brought into Eq. (2) to calculate the next-generation population.

$$\begin{aligned}
 O_{p+1,q,r} = & O_{p,q,r} + \alpha_{p,q,1}(O_{p,q,best} - \text{abs}(O_{p,q,r})) \\
 & - \alpha_{p,q,2}(O_{p,q,worst} - \text{abs}(O_{p,q,r}))
 \end{aligned}
 \tag{2}$$

where  $p$ ,  $q$ , and  $r$  are the index of iteration, variable, and candidate solution.  $O_{p,q,r}$  denotes the  $q$ th variable of the  $r$ th candidate solution of the  $p$ th iteration.  $\alpha_{p,q,1}$  and  $\alpha_{p,q,2}$  are random numbers between 0 and 1 that act as scaling factors,

together with the absolute values of the variables to ensure that the exploration of the algorithm can proceed properly.  $O_{p,q,best}$  and  $O_{p,q,worst}$  denote the  $q$ th variable of the best and worst solution in the  $p$ th iteration, respectively.

All the solutions are combined with the initial population to form a set of solutions of size  $2P$  ( $P$  is the size of the initial population) after being updated. Recalculate the non-dominated rank and crowding distance  $\xi$  of  $2P$  solutions and select  $P$  outstanding solution sets from them to be computed in the next iteration. This feature selection ensures that only the superior solution is retained for each iteration of the MO-Jaya algorithm. As the set of non-dominated solutions increases, the algorithm ensures that it always moves towards the Pareto optimum and eventually converges to the Pareto front.

#### 3.2.1 Non-dominated sorting

The ranking is based on the non-dominated relationship between the solutions. For an  $M$ -objective optimization problem,  $P$  is the set of solutions to be ordered. A solution  $x_1$  is said to dominate another solution  $x_2$  if and only if  $f_i(x_1) \leq f_i(x_2)$  for all  $1 \leq i \leq M$  and  $f_i(x_1) < f_i(x_2)$  for at least one  $i$ , where  $i \in \{1, \dots, M\}$ . A solution  $x^*$  in  $P$  is non-dominated if there does not exist any solution  $x_j$  in  $P$  that dominates  $x^*$ . Assign  $x^*$  a non-dominant rank of 1 (rank = 1). Next, eliminate  $x^*$  (rank = 1) from the set of all solutions, re-determine the dominance relationship for the remaining individuals, and so on, until all non-dominance ranks are found. A set of solutions with the same rank is known as the front ( $F$ ).

#### 3.2.2 Computing the crowding distance

To compare the superiority of solutions of the same non-dominated rank, the crowding distance  $\xi_j$  is brought up. It is a measure of the density estimate of solutions near a particular solution  $j$ . For a particular front  $F$ , let  $l = |F|$ , and for each solution in  $F$ , the crowding distance  $\xi$  is computed as follows:

- Step 1: Initialize  $\xi_j = 0$ .
- Step 2: Sort the solutions in  $F$  by the  $m$ th optimization objective value  $f_m$ .
- Step 3: In the sorted list of  $m$ th objective, assign infinite crowding distance to solutions at the extremes of the sorted list (i.e.,  $\xi_1 = \xi_l = \infty$ ), for  $j = 2$  to  $(l - 1)$ , calculate  $\xi_j$  as follows. It is worth noting that the calculated crowding distance needs to be normalized.

**Table 3** Box-Behnken response surface design matrix and experimental results

| Std | Run | $P$ | $a$ | $D$ | $\alpha$ | $u$ | $S$ | $h$ ( $\mu\text{m}$ ) | ( $\text{mm}^3/\text{s}$ ) | $Ra_x$ ( $\mu\text{m}$ ) |
|-----|-----|-----|-----|-----|----------|-----|-----|-----------------------|----------------------------|--------------------------|
| 47  | 1   | -1  | 0   | 1   | 0        | 0   | 1   | 540.281               | 207.141                    | 26.067                   |
| 16  | 2   | 0   | 1   | 1   | 0        | 1   | 0   | 774.825               | 316.198                    | 34.319                   |
| 20  | 3   | 0   | 0   | 1   | 1        | 0   | -1  | 1392.488              | 262.638                    | 73.758                   |
| 29  | 4   | -1  | 0   | 0   | -1       | 1   | 0   | 420.452               | 208.667                    | 17.865                   |
| 3   | 5   | -1  | 1   | 0   | -1       | 0   | 0   | 747.080               | 256.080                    | 44.508                   |
| 22  | 6   | 0   | 0   | 1   | -1       | 0   | 1   | 596.839               | 266.823                    | 42.205                   |
| 46  | 7   | 1   | 0   | -1  | 0        | 0   | 1   | 862.869               | 282.569                    | 114.263                  |
| 14  | 8   | 0   | 1   | -1  | 0        | 1   | 0   | 761.956               | 341.665                    | 61.532                   |
| 23  | 9   | 0   | 0   | -1  | 1        | 0   | 1   | 571.919               | 219.933                    | 46.163                   |
| 6   | 10  | 1   | -1  | 0   | 1        | 0   | 0   | 565.010               | 163.899                    | 36.805                   |
| 38  | 11  | 0   | 1   | 0   | 0        | -1  | 1   | 1322.237              | 321.791                    | 132.794                  |
| 32  | 12  | 1   | 0   | 0   | 1        | 1   | 0   | 735.853               | 318.472                    | 57.498                   |
| 53  | 13  | 0   | 0   | 0   | 0        | 0   | 0   | 1095.268              | 271.243                    | 62.236                   |
| 8   | 14  | 1   | 1   | 0   | 1        | 0   | 0   | 1342.649              | 384.151                    | 97.960                   |
| 25  | 15  | -1  | 0   | 0   | -1       | -1  | 0   | 1082.765              | 228.388                    | 71.319                   |
| 30  | 16  | 1   | 0   | 0   | -1       | 1   | 0   | 660.382               | 345.959                    | 62.579                   |
| 40  | 17  | 0   | 1   | 0   | 0        | 1   | 1   | 535.919               | 289.315                    | 45.862                   |
| 35  | 18  | 0   | -1  | 0   | 0        | 1   | -1  | 517.204               | 145.758                    | 23.454                   |
| 44  | 19  | 1   | 0   | 1   | 0        | 0   | -1  | 1796.323              | 349.625                    | 74.657                   |
| 52  | 20  | 0   | 0   | 0   | 0        | 0   | 0   | 990.064               | 271.373                    | 61.469                   |
| 17  | 21  | 0   | 0   | -1  | -1       | 0   | -1  | 1190.179              | 308.694                    | 60.423                   |
| 49  | 22  | 0   | 0   | 0   | 0        | 0   | 0   | 959.221               | 274.134                    | 65.572                   |
| 51  | 23  | 0   | 0   | 0   | 0        | 0   | 0   | 944.950               | 273.361                    | 60.417                   |
| 33  | 24  | 0   | -1  | 0   | 0        | -1  | -1  | 1278.576              | 161.072                    | 54.977                   |
| 4   | 25  | 1   | 1   | 0   | -1       | 0   | 0   | 1260.135              | 413.683                    | 84.302                   |
| 13  | 26  | 0   | -1  | -1  | 0        | 1   | 0   | 334.266               | 133.591                    | 32.493                   |
| 48  | 27  | 1   | 0   | 1   | 0        | 0   | 1   | 764.475               | 314.384                    | 51.111                   |
| 12  | 28  | 0   | 1   | 1   | 0        | -1  | 0   | 1905.496              | 334.882                    | 80.605                   |
| 31  | 29  | -1  | 0   | 0   | 1        | 1   | 0   | 465.394               | 168.638                    | 22.288                   |
| 43  | 30  | -1  | 0   | 1   | 0        | 0   | -1  | 1066.014              | 226.284                    | 47.324                   |
| 41  | 31  | -1  | 0   | -1  | 0        | 0   | -1  | 1108.616              | 225.081                    | 68.032                   |
| 27  | 32  | -1  | 0   | 0   | 1        | -1  | 0   | 1240.142              | 212.773                    | 68.759                   |
| 19  | 33  | 0   | 0   | -1  | 1        | 0   | -1  | 1598.606              | 268.353                    | 88.437                   |
| 36  | 34  | 0   | 1   | 0   | 0        | 1   | -1  | 1259.822              | 335.288                    | 65.685                   |
| 2   | 35  | 1   | -1  | 0   | -1       | 0   | 0   | 543.900               | 171.190                    | 46.897                   |
| 26  | 36  | 1   | 0   | 0   | -1       | -1  | 0   | 1830.259              | 354.477                    | 62.353                   |
| 7   | 37  | -1  | 1   | 0   | 1        | 0   | 0   | 789.345               | 217.700                    | 37.551                   |
| 50  | 38  | 0   | 0   | 0   | 0        | 0   | 0   | 1015.509              | 272.742                    | 52.069                   |
| 39  | 39  | 0   | -1  | 0   | 0        | 1   | 1   | 256.990               | 133.473                    | 23.997                   |
| 5   | 40  | -1  | -1  | 0   | 1        | 0   | 0   | 352.542               | 97.439                     | 28.649                   |
| 28  | 41  | 1   | 0   | 0   | 1        | -1  | 0   | 1981.079              | 331.921                    | 108.182                  |
| 42  | 42  | 1   | 0   | -1  | 0        | 0   | -1  | 1927.778              | 336.197                    | 113.702                  |
| 24  | 43  | 0   | 0   | 1   | 1        | 0   | 1   | 586.852               | 223.975                    | 24.594                   |
| 1   | 44  | -1  | -1  | 0   | -1       | 0   | 0   | 313.599               | 104.494                    | 17.712                   |
| 45  | 45  | -1  | 0   | -1  | 0        | 0   | 1   | 476.025               | 165.088                    | 62.531                   |
| 18  | 46  | 0   | 0   | 1   | -1       | 0   | -1  | 1362.920              | 328.218                    | 31.372                   |
| 9   | 47  | 0   | -1  | -1  | 0        | -1  | 0   | 1031.880              | 171.168                    | 69.450                   |
| 11  | 48  | 0   | -1  | 1   | 0        | -1  | 0   | 1107.110              | 186.602                    | 49.368                   |
| 54  | 49  | 0   | 0   | 0   | 0        | 0   | 0   | 1194.844              | 310.151                    | 55.812                   |
| 37  | 50  | 0   | -1  | 0   | 0        | -1  | 1   | 798.695               | 166.637                    | 66.535                   |
| 10  | 51  | 0   | 1   | -1  | 0        | -1  | 0   | 2307.513              | 393.147                    | 121.713                  |

**Table 3** (continued)

| Std | Run | $P$ | $a$ | $D$ | $\alpha$ | $u$ | $S$ | $h$ ( $\mu\text{m}$ ) | ( $\text{mm}^3/\text{s}$ ) | $Ra_x$ ( $\mu\text{m}$ ) |
|-----|-----|-----|-----|-----|----------|-----|-----|-----------------------|----------------------------|--------------------------|
| 34  | 52  | 0   | 1   | 0   | 0        | -1  | -1  | 3571.845              | 399.146                    | 56.152                   |
| 21  | 53  | 0   | 0   | -1  | -1       | 0   | 1   | 612.805               | 268.203                    | 41.708                   |
| 15  | 54  | 0   | -1  | 1   | 0        | 1   | 0   | 422.032               | 165.891                    | 26.988                   |

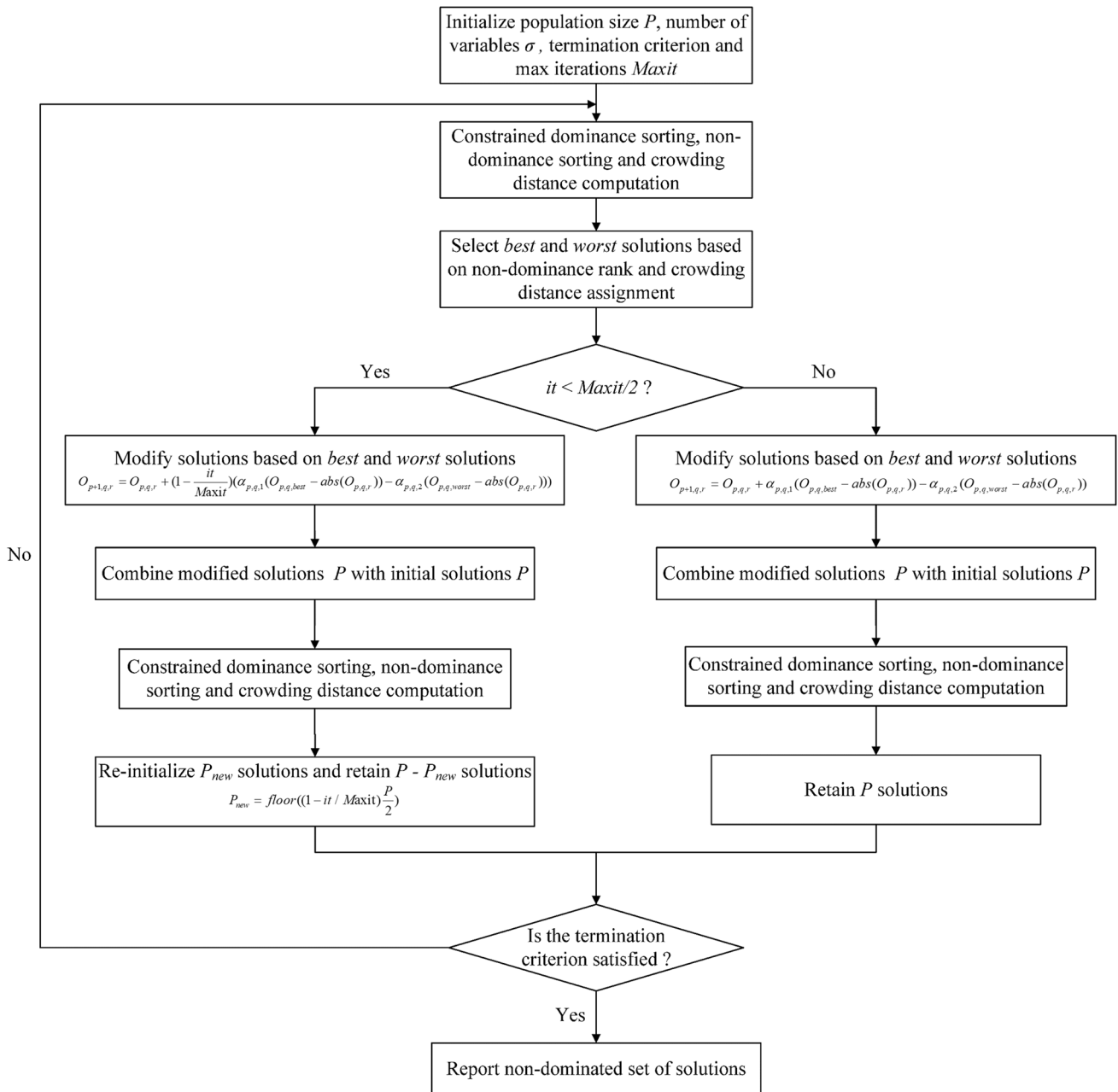


**Fig. 4** Flowchart for ADM-MO-Jaya algorithm

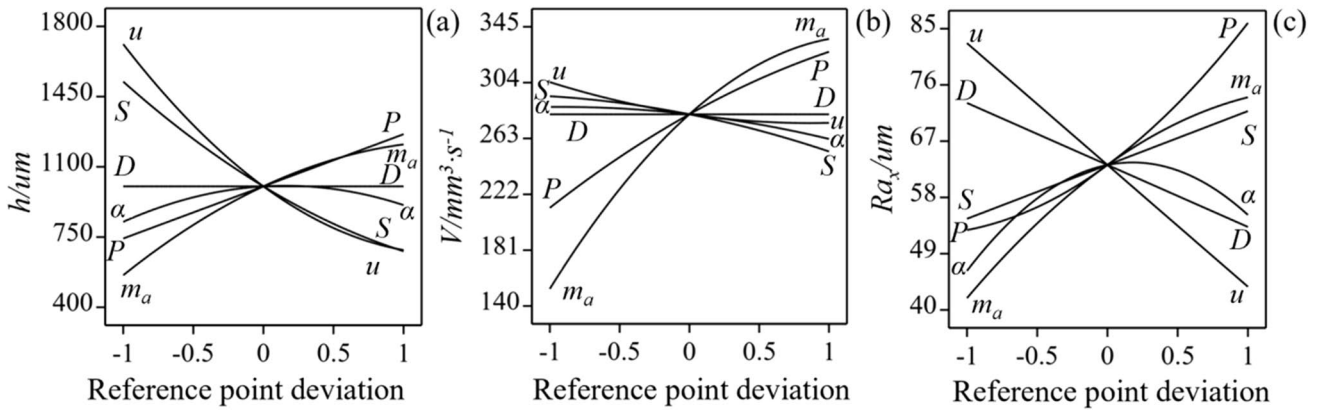


Fig. 5 Perturbation diagram of process parameters on **a**  $h$ , **b**  $\dot{V}$ , and **c**  $Ra_x$

$$\xi_j = \xi_j + \frac{f_m^{j+1} - f_m^{j-1}}{f_m^{max} - f_m^{min}} \quad (3)$$

Step 4: Iterate through all objectives and calculate the solution set crowding distance for each optimization objective according to steps 1–3, respectively. The crowding

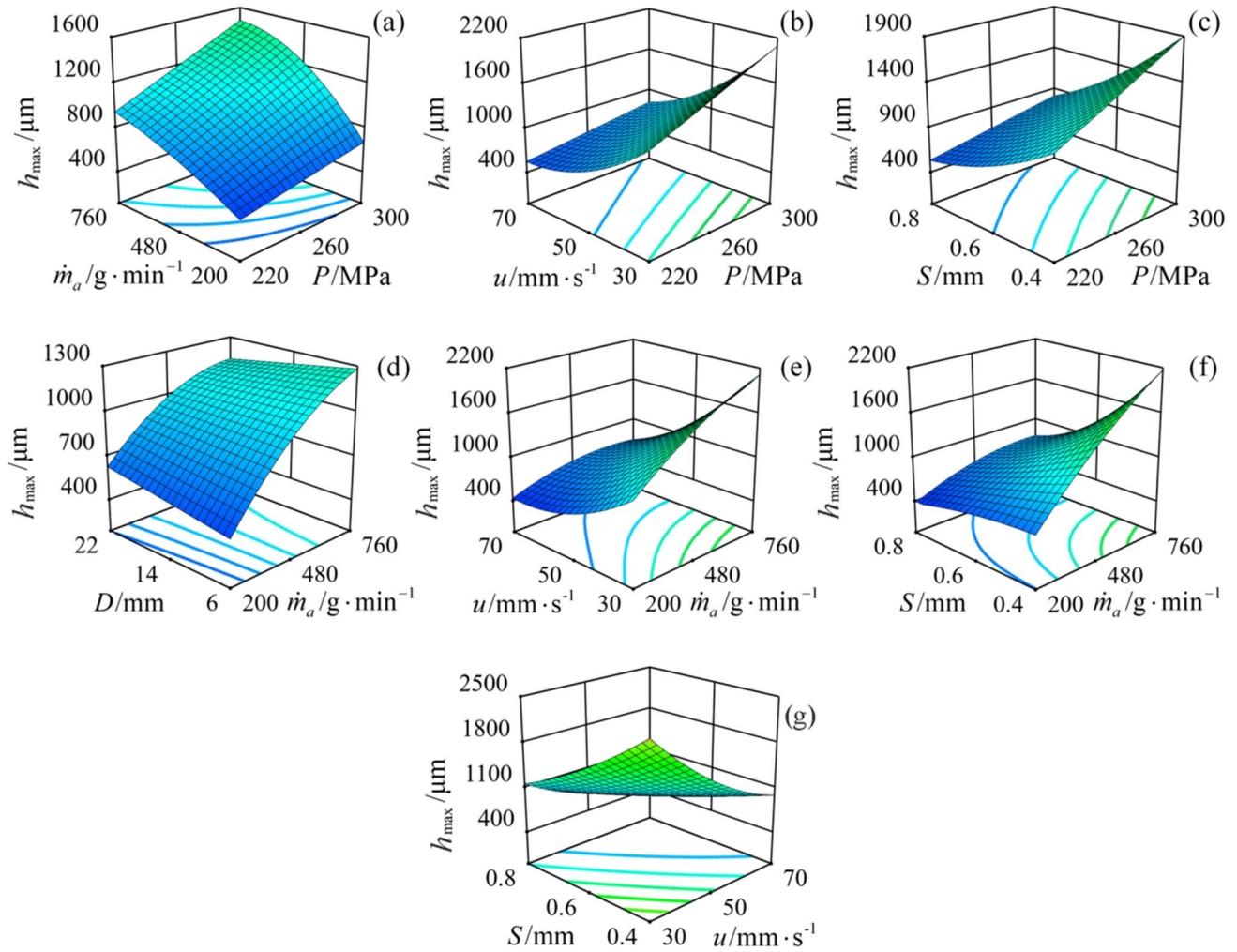
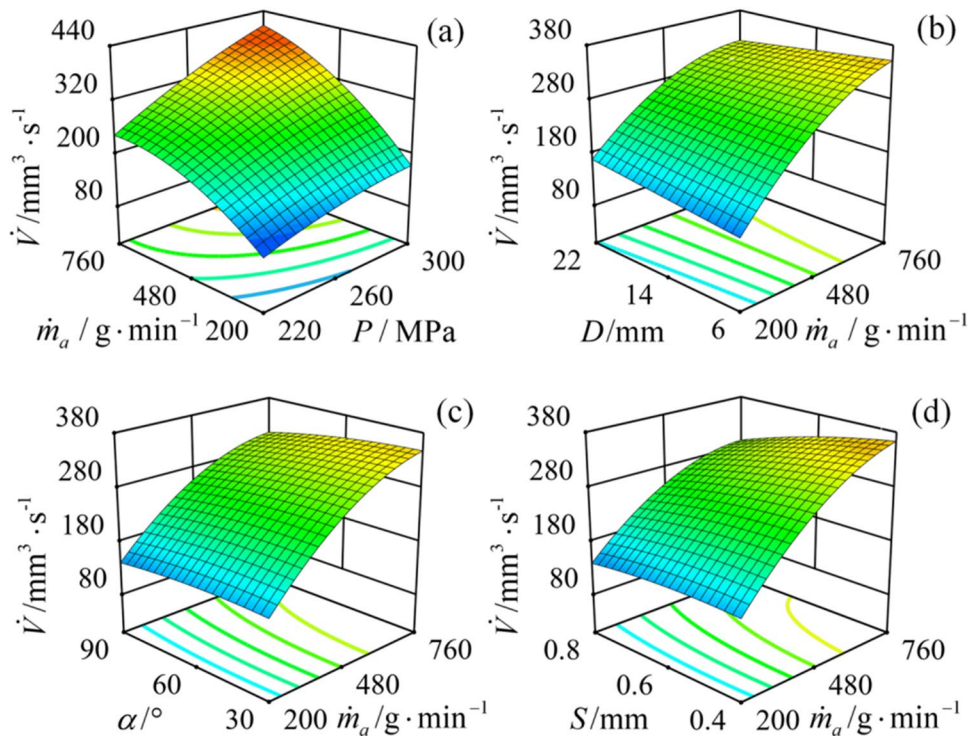


Fig. 6 Effect of interaction of process parameters on  $h$ ; **a**  $\dot{m}_a$  and  $P$ ; **b**  $u$  and  $P$ ; **c**  $S$  and  $P$ ; **d**  $D$  and  $\dot{m}_a$ ; **e**  $u$  and  $\dot{m}_a$ ; **f**  $S$  and  $\dot{m}_a$ ; **g**  $S$  and  $u$



**Fig. 7** Effect of interaction of process parameters on  $\dot{V}$ ; **a** the interaction of  $\dot{m}_a$  and  $P$ ; **b** the interaction of  $D$  and  $\dot{m}_a$ ; **c** the interaction of  $\alpha$  and  $\dot{m}_a$ ; **f** the interaction of  $S$  and  $\dot{m}_a$



distances under different objectives are then summed to be the crowding of the solution set under the front  $F$ .

**3.3 ADM-MO-Jaya algorithm**

The MO-Jaya algorithm iterates according to Eq. (2) after one initialization. Unlike the genetic algorithm, there is no complex mutation operation, and easy to fall into the local optimum. Therefore, in this paper, the total number of iterations is divided into two parts, and when the number of iterations is less than half of the total number of iterations, some populations are re-initialized every certain number of iterations to increase the population diversity and improve the searchability of the algorithm. The flowchart of the ADM-MO-Jaya optimization algorithm is shown in Fig. 4. To avoid that re-initializing some populations would reduce

the convergence speed, an adaptive decreasing method was adopted to initialize the number of populations.

$$P_{new} = \text{floor}((1 - it/\text{Maxit})\frac{P}{2}) \tag{4}$$

where  $P$  is the initial population capacity, and  $P_{new}$  is the re-initialized population capacity. The original MO-Jaya algorithm retains  $P$  individuals each time to the next iteration. Now, for every certain number of iterations,  $P - P_{new}$  optimal individuals are retained, while  $P_{new}$  individuals are initialized to form a population of  $P$  individuals into the computation.  $it$  is the current number of iterations, and  $\text{Maxit}$  is the total number of iterations. As  $it$  increases, the number of  $P_{new}$  decreases gradually from  $P/2$ .

When the ADM-MO-Jaya algorithm is run for the latter stage, the next generation population generated according

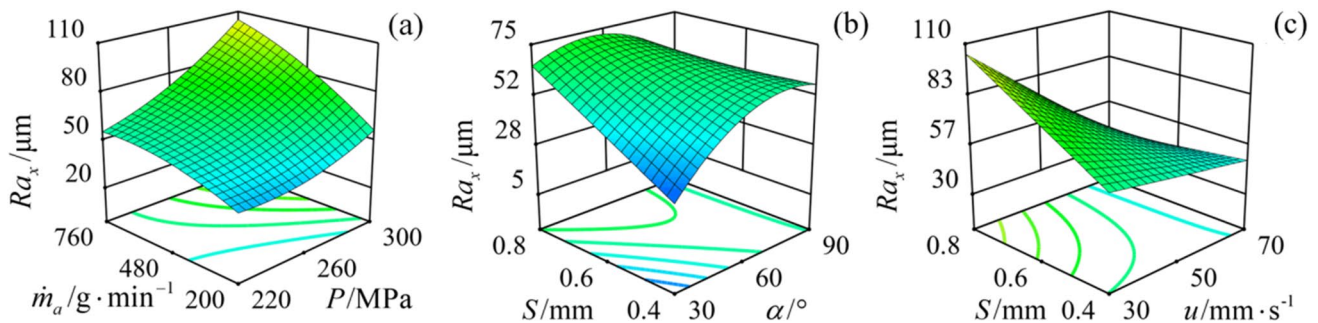


**Fig. 8** Effect of interaction of process parameters on  $Ra_x$ ; **a**  $\dot{m}_a$  and  $P$ ; **b**  $S$  and  $\alpha$ ; **c**  $S$  and  $u$

to Eq. (2) may cause repeated changes in the offspring population due to excessive step size. As a result, it cannot converge to the uniform Pareto front. Therefore, when  $it$  is greater than  $Maxit/2$ , the algorithm introduces an adaptive reduction of the step to improve the convergence of the algorithm. As shown in Eq. (5), with the increase of  $it$ , the step length increased by  $O_{p,q,r}$  will gradually decrease, and the convergence accuracy of the algorithm will be higher.

$$O_{p+1,q,r} = O_{p,q,r} + (1 - \frac{it}{Maxit})(\alpha_{p,q,1}(O_{p,q,best} - abs(O_{p,q,r})) - \alpha_{p,q,2}(O_{p,q,worst} - abs(O_{p,q,r}))) \tag{5}$$

## 4 Results and discussion

### 4.1 Influence of process parameters on the milling characteristics

#### 4.1.1 Influence of single process parameters

Figure 5 shows the perturbation diagram of process parameters on  $h$ ,  $\dot{V}$ , and  $Ra_x$ . As illustrated in Fig. 5a,  $h$  is strongly affected by  $u$  and negatively correlated with  $u$ . When  $u$

increases, there is a drop in the erosion time, resulting in the decrease of  $h$ . The effect of the  $S$  on  $h$  is consistent with that of  $u$ , which is because the increased  $S$  shrinks the jet overlap area. However, the relationship between  $h$  and  $\dot{m}_a$  is positive. A deeper  $h$  can be obtained when  $\dot{m}_a$  is larger; this can be attributed to the fact that more abrasive grains can erode the target material per unit of time. Typically, the increase of  $\dot{m}_a$  also leads to enhanced abrasive interference, so the increasing trend gradually decreases. Notably, the  $h$  is almost independent of the  $D$  but has a linear positive correlation with the  $P$ , indicating that the change of jet energy caused by  $P$  is larger than that of  $D$  within a given parameter range. As the  $\alpha$  increases, the  $h$  first increases and then decreases, this is due to the combined effect of shear energy, impact energy, and jet hysteresis.

It can be found from Fig. 5b that  $\dot{m}_a$  has the most significant effect on the  $\dot{V}$ , followed by  $P$ ,  $\alpha$ ,  $S$ , and  $u$ ; the influence of  $D$  on  $\dot{V}$  is slightest. It is that  $\dot{m}_a$  getting larger with  $\dot{V}$  keeps increasing but the trend gradually slows down. This is because more abrasive particles will erode the target material per unit time in turn cause a higher  $\dot{V}$ . Similar phenomenon also occurs in the effect of  $P$  on  $\dot{V}$ . A larger  $P$  contributes to higher kinetic energy of the abrasive particles impacting the target material, resulting in an increase in  $\dot{V}$ .

**Table 4** ANOVA results of  $h$

| Source          | Sum of squares | df | Mean square | F-value | P-value |
|-----------------|----------------|----|-------------|---------|---------|
| Model           | 1.857E+007     | 18 | 1.032E+006  | 116.68  | <0.0001 |
| $P$             | 1.339E+006     | 1  | 1.339E+006  | 151.42  | <0.0001 |
| $\dot{m}_a$     | 1.702E+006     | 1  | 1.702E+006  | 192.52  | <0.0001 |
| $a$             | 41,713.68      | 1  | 41,713.68   | 4.72    | 0.0367  |
| $u$             | 6.317E+006     | 1  | 6.317E+006  | 714.41  | <0.0001 |
| $S$             | 4.288E+006     | 1  | 4.288E+006  | 484.97  | <0.0001 |
| $P \dot{m}_a$   | 48,608.06      | 1  | 48,608.06   | 5.50    | 0.0248  |
| $Pu$            | 1.196E+005     | 1  | 1.196E+005  | 13.52   | 0.0008  |
| $PS$            | 1.101E+005     | 1  | 1.101E+005  | 12.45   | 0.0012  |
| $\dot{m}_a D$   | 38,107.87      | 1  | 38,107.87   | 4.31    | 0.0453  |
| $\dot{m}_a u$   | 5.963E+005     | 1  | 5.963E+005  | 67.44   | <0.0001 |
| $\dot{m}_a S$   | 6.235E+005     | 1  | 6.235E+005  | 70.52   | <0.0001 |
| $uS$            | 3.808E+005     | 1  | 3.808E+005  | 43.07   | <0.0001 |
| $\dot{m}_a^2$   | 1.460E+005     | 1  | 1.460E+005  | 16.51   | 0.0003  |
| $a^2$           | 2.127E+005     | 1  | 2.127E+005  | 24.05   | <0.0001 |
| $u^2$           | 4.088E+005     | 1  | 4.088E+005  | 46.24   | <0.0001 |
| $S^2$           | 1.149E+005     | 1  | 1.149E+005  | 13.00   | 0.0010  |
| $\dot{m}_a uS$  | 2.132E+005     | 1  | 2.132E+005  | 24.12   | <0.0001 |
| $\dot{m}_a S^2$ | 1.259E+005     | 1  | 1.259E+005  | 14.24   | 0.0006  |
| Residual        | 3.095E+005     | 35 | 8841.63     |         |         |
| Lack of fit     | 2.640E+005     | 30 | 8801.37     | 0.97    | 0.5831  |
| Pure error      | 45,415.79      | 5  | 9083.16     |         |         |
| Cor total       | 1.888E+007     | 53 |             |         |         |
| $R^2=0.9836$    |                |    |             |         |         |

**Table 5** ANOVA results of  $\dot{V}$

| Source        | Sum of squares | df | Mean square | F-value | P-value |
|---------------|----------------|----|-------------|---------|---------|
| Model         | 3.367E+005     | 17 | 19804.77    | 174.64  | <0.0001 |
| $P$           | 52,485.78      | 1  | 52,485.78   | 462.82  | <0.0001 |
| $\dot{m}_a$   | 2.020E+005     | 1  | 2.020E+005  | 1781.27 | <0.0001 |
| $a$           | 4853.05        | 1  | 4853.05     | 42.79   | <0.0001 |
| $u$           | 5372.70        | 1  | 5372.70     | 47.38   | <0.0001 |
| $S$           | 9882.93        | 1  | 9882.93     | 87.15   | <0.0001 |
| $P \dot{m}_a$ | 4555.26        | 1  | 4555.26     | 40.17   | <0.0001 |
| $\dot{m}_a D$ | 2160.41        | 1  | 2160.41     | 19.05   | 0.0001  |
| $\dot{m}_a a$ | 358.66         | 1  | 358.66      | 3.16    | 0.0838  |
| $\dot{m}_a S$ | 1699.68        | 1  | 1699.68     | 14.99   | 0.0004  |
| $P^2$         | 1368.21        | 1  | 1368.21     | 12.06   | 0.0014  |
| $\dot{m}_a^2$ | 13,931.02      | 1  | 13,931.02   | 122.84  | <0.0001 |
| $a^2$         | 424.27         | 1  | 424.27      | 3.74    | 0.0610  |
| $u^2$         | 787.02         | 1  | 787.02      | 6.94    | 0.0123  |
| $S^2$         | 549.87         | 1  | 549.87      | 4.85    | 0.0342  |
| $P^2D$        | 979.01         | 1  | 979.01      | 8.63    | 0.0057  |
| $P^2a$        | 885.23         | 1  | 885.23      | 7.81    | 0.0083  |
| $Pu^2$        | 458.40         | 1  | 458.40      | 4.04    | 0.0519  |
| Residual      | 4082.54        | 36 | 113.40      |         |         |
| Lack of fit   | 2899.34        | 31 | 93.53       | 0.40    | 0.9505  |
| Pure error    | 1183.20        | 5  | 236.64      |         |         |
| Cor total     | 3.408E+005     | 53 |             |         |         |
| $R^2=0.9880$  |                |    |             |         |         |

As shown in Fig. 5c,  $Ra_x$  is most sensitive to the change of  $u$  compared with other parameters, and it decreases linearly with the increase of  $u$ . Similarly,  $D$  has a negative effect on  $Ra_x$ . Inversely,  $P$  and  $\dot{m}_a$  have positive impacts on  $Ra_x$ . The  $Ra_x$  increases gradually with the increase of  $S$ , which is because the overlap region of the jet trajectory plays an important role in material erosion. When the overlap area increases, there will be unmachined positions between two adjacent milling paths, and therefore the  $Ra_x$  will be relatively larger.

**4.1.2 The interactive effects of process parameters**

The response surface method was used to obtain the effect of the process parameters’ interactions on the milling characteristics. Figures 6, 7, and 8 show the response surface contour of the interactive effect between two parameters.

From Fig. 6a, b, and c, it can be claimed that a greater  $h$  can be obtained only when the  $P$  is larger, the  $u$  and  $S$  are smaller or the  $\dot{m}_a$  is larger. Figure 6d, e, and f shows that larger  $h$  can be acquired at the conditions of larger  $\dot{m}_a$  and smaller  $D$ ,  $u$ , or  $S$ . As exhibited in Fig. 6g, a larger  $h$  can be gained at smaller  $S$  and  $u$ . All the results are consistent with the previous single factor’s effects on  $h$ .

As illustrated in Fig. 7, the effects of the interaction between process parameters on the  $\dot{V}$  are explored. From Fig. 7a, it can be seen that a larger  $\dot{V}$  is obtained after a larger  $\dot{m}_a$  is taken when the  $P$  is higher. Figure 7b, c, and d shows that it is necessary for a higher  $\dot{m}_a$  combined with lower  $D$ ,  $\alpha$ , or  $S$  in order to get larger  $\dot{V}$ . The effect of interaction between  $P$  and  $\dot{m}_a$  on the  $\dot{V}$  is obvious, which is mainly due to the fact that the increase in  $P$  and  $\dot{m}_a$  leads to an increase in the kinetic energy of the abrasive, resulting in a stronger erosive effect on the material and therefore a greater  $\dot{V}$  can be obtained.

The effect of the interaction between the process parameters on  $Ra_x$  is depicted in Fig. 8. In Fig. 8a, a smaller  $\dot{m}_a$  yields a lower  $Ra_x$  when the  $P$  is smaller. Figure 8b, c shows that a smaller  $\alpha$  or a larger  $u$  is required to obtain a lower  $Ra_x$  when the  $S$  is smaller. This is mainly because the reduction of  $P$  and  $\dot{m}_a$  will reduce the abrasive erosion on the material, the larger  $u$  will reduce the jet dwell time, the smaller  $S$  will eliminate the abrupt peaks between the multiple milling paths, and the reduction of  $\alpha$  allows the abrasive to shift from vertical erosion to slip rubbing along the path so that a smaller roughness can be obtained.

**4.2 Regression analysis**

Regression analysis was performed on the results of response surface analysis, and the cubic regression model of  $h$ ,  $\dot{V}$ , and  $Ra_x$  were obtained (Eqs. 6, 7, and 8). All six input process parameters in the regression model range from  $-1$  to  $1$ , resulting from the Box–Behnken design method.

$$h = 1002.59448 + 236.18571P + 326.16625\dot{m}_a + 41.69017a - 513.02092u - 422.68604S + 77.94875P\dot{m}_a - 122.25525Pu - 117.30413PS - 69.01800\dot{m}_aD - 193.05000\dot{m}_au - 279.17700\dot{m}_aS + 218.17150aS - 116.98358\dot{m}_a^2 - 135.18574a^2 + 195.77467u^2 + 99.38195S^2 + 163.25475\dot{m}_auS + 153.62850\dot{m}_aS^2 \tag{6}$$

$$\dot{V} = 280.75674 + 57.27444P + 91.74300ma - 24.62987a - 14.96204u - 20.29258S + 23.86225P\dot{m}_a - 16.43325\dot{m}_aD - 6.69575\dot{m}_a a - 14.57600\dot{m}_aS - 11.41514P^2 - 36.42477m_a^2 - 6.35664a^2 + 8.65761u^2 - 7.00684S^2 + 11.06237P^2D + 12.88331P^2a + 9.27094Pu^2 \tag{7}$$

$$Ra_x = 60.19811 + 16.57100P + 16.06908\dot{m}_a - 9.91937D + 4.47504a - 19.48529u - 9.31644S + 7.85775P\dot{m}_a - 10.44450aS - 13.43500uS + 6.90533P^2 - 11.72304a^2 - 7.23663Pau - 10.68125\dot{m}_auS - 10.00175P^2D + 17.93144\dot{m}_aS \tag{8}$$

Tables 4, 5, and 6 show the coefficient statistics and ANOVA results of the three models of  $h$ ,  $\dot{V}$ , and  $Ra_x$ , where a larger  $F$ -value means that the factor has a greater influence on the results of the test. The effect of all models and each model item were relatively significant, and the effect of the misfit term was not significant according to the statistical evaluation criteria ( $P \leq \alpha = 0.05$ ). The correlation coefficients  $R^2$  of the models are 0.9836, 0.9830, and 0.9049, respectively. Since the correlation coefficients are all greater

**Table 6** ANOVA results of  $Ra_x$

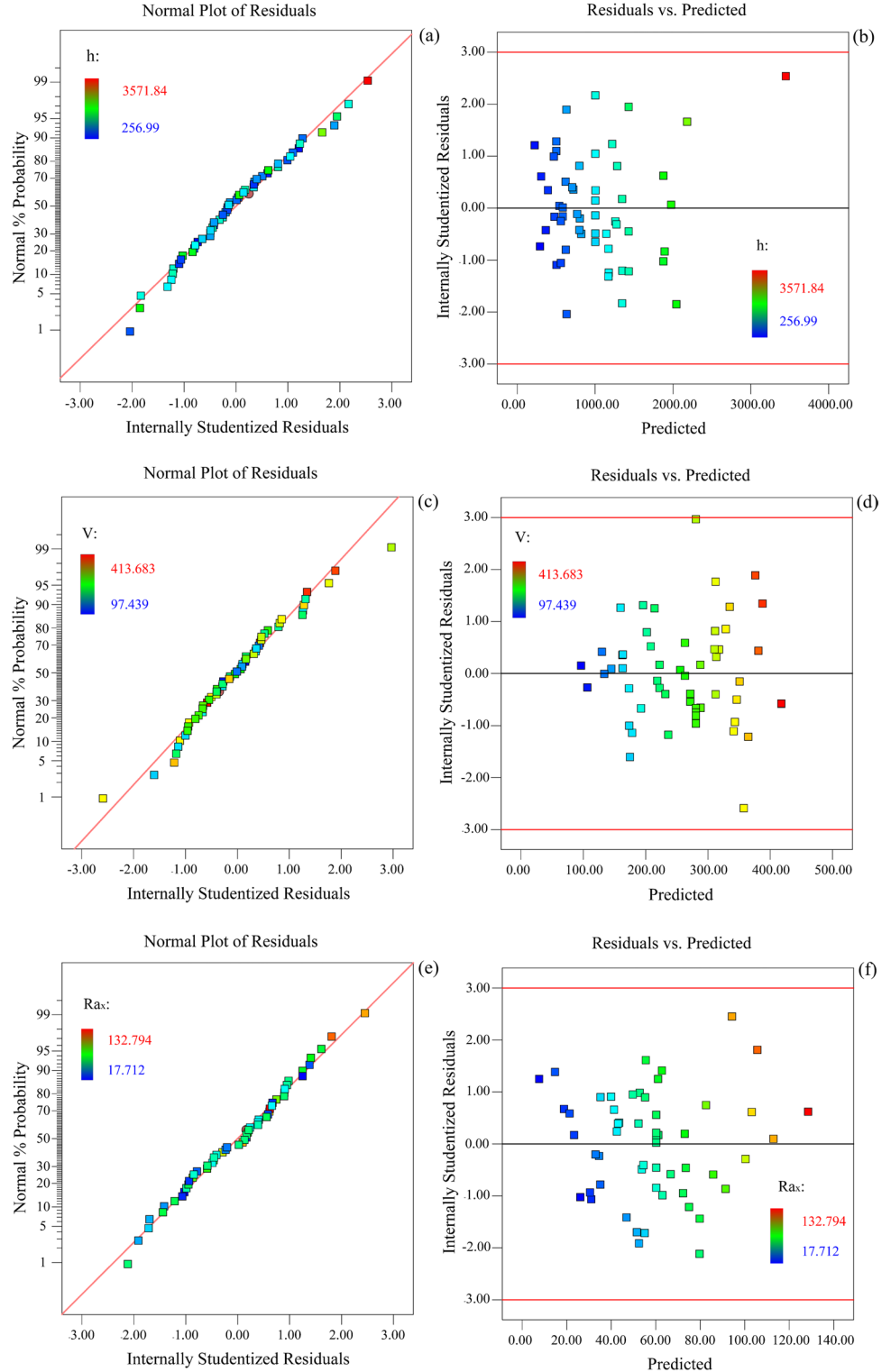
| Source         | Sum of squares | df | Mean square | F-value | P-value |
|----------------|----------------|----|-------------|---------|---------|
| Model          | 34,858.99      | 15 | 2323.93     | 24.11   | <0.0001 |
| $P$            | 6590.35        | 1  | 6590.35     | 68.36   | <0.0001 |
| $\dot{m}_a$    | 6197.17        | 1  | 6197.17     | 64.28   | <0.0001 |
| $D$            | 1574.30        | 1  | 1574.30     | 16.33   | 0.0002  |
| $a$            | 480.62         | 1  | 480.62      | 4.99    | 0.0315  |
| $u$            | 9112.24        | 1  | 9112.24     | 94.52   | <0.0001 |
| $S$            | 1388.74        | 1  | 1388.74     | 14.41   | 0.0005  |
| $P\dot{m}_a$   | 493.95         | 1  | 493.95      | 5.12    | 0.0294  |
| $aS$           | 872.70         | 1  | 872.70      | 9.05    | 0.0046  |
| $uS$           | 1443.99        | 1  | 1443.99     | 14.98   | 0.0004  |
| $P^2$          | 534.06         | 1  | 534.06      | 5.54    | 0.0239  |
| $a^2$          | 1539.21        | 1  | 1539.21     | 15.97   | 0.0003  |
| $Pau$          | 418.95         | 1  | 418.95      | 4.35    | 0.0439  |
| $\dot{m}_auS$  | 912.71         | 1  | 912.71      | 9.47    | 0.0039  |
| $P^2D$         | 533.52         | 1  | 533.52      | 5.53    | 0.0239  |
| $\dot{m}_a^2S$ | 1714.86        | 1  | 1714.86     | 17.79   | 0.0001  |
| Residual       | 3663.35        | 38 | 96.40       |         |         |
| Lack of fit    | 3545.51        | 33 | 107.44      | 4.56    | 0.1646  |
| Pure error     | 117.84         | 5  | 23.57       |         |         |
| Cor total      | 38,522.34      | 53 |             |         |         |
| $R^2 = 0.9049$ |                |    |             |         |         |

than 0.9, the reliability of the regression models is good, and the modeling is valid.

The residual normal probability distributions of  $h$ ,  $\dot{V}$ , and  $Ra_x$  are shown in Fig. 9a, c, and e, respectively. Figure 9b, d, and f shows the relationships between model residual

of  $h$ ,  $\dot{V}$ ,  $Ra_x$  and the predicted response. The points on the residual normal probability plot of all models are essentially on a straight line, indicating that the residuals obey a normal distribution. It can be seen that the residuals of all models

**Fig. 9** Regression model residuals normal distribution and predicted response; **a** normal residual of  $h$ , **b** residual vs. predicted of  $h$ , **c** normal residual of  $\dot{V}$ , **d** Residual vs. predicted of  $\dot{V}$ , **e** normal residual of  $Ra_x$ , and **f** residual vs. predicted of  $Ra_x$



meet the random distribution without anomalous structures or obvious patterns. It indicates that there is no regularity between the residuals and the predicted values, and the nonrandom error of the experimental data is not significant. Thus, it can be demonstrated the above regression models are all correct and credible.

A total of 30 sets of milling experiments were used to assess the generalization ability of the model. Figure 10 shows the predicted and experimental values of  $h$ ,  $\dot{V}$ , and  $Ra_x$ . As can be seen from the figure, the predicted values of the  $h$ ,  $\dot{V}$ , and  $Ra_x$  regression models are highly consistent with the overall trend of the experimental values, although there are several errors in some data points. The coincidence between predicted and experimental values  $\dot{V}$  is surprisingly high compared with  $h$  and  $Ra_x$ .

The mean errors between the experimental and predicted values of  $h$ ,  $\dot{V}$ , and  $Ra_x$  were 8.57%, 1.89%, and 10.58%, respectively. The average error of all three models is smaller than that of the existing literature [29–31]. Considering the pressure fluctuation, abrasive distribution, vibration, etc., the above models can be considered to have a fairly good generalization capability.

### 4.3 Multi-objective optimization

The regression model developed in this paper can accurately map the relationship between process parameters and  $h$ ,  $\dot{V}$ , and  $Ra_x$ . However, it is equally important to determine the combination of input process parameters to obtain the best surface roughness and machining efficiency. Therefore, three optimization algorithms, NSGA-II, MO-Jaya, and ADM-MO-Jaya, were introduced for multi-objective optimization of  $h$ ,  $\dot{V}$ , and  $Ra_x$  to obtain the maximum  $h$ ,  $\dot{V}$ , and the minimum  $Ra_x$  based on the above regression models. Given that the optimization algorithm generally aims to obtain the minimum value, adding negative signs to the  $h$  and  $\dot{V}$ . All algorithms were implemented on MATLAB R2021a; the computer CPU is Intel i5 12400F. The population size of all three algorithms was set to 180, and the maximum number of iterations is 2000. Each algorithm is run 10 times to evaluate its efficiency.

As can be seen in Fig. 11, all three algorithms converge to the Pareto front, exhibiting good convergence ability. Among them, the Pareto front optimized by the classical NSGA-II algorithm is uniform and converges to a curve in the solution space. However, there are several isolated points, and the part of  $Ra_x$  greater than 80  $\mu\text{m}$  is not fully converged. As for the MO-Jaya algorithm, it has the worst convergence and it is difficult to converge when the  $Ra_x$  is greater than 80  $\mu\text{m}$ . Moreover, there are several isolated points at other locations. It is of great interest to find that the Pareto front optimized by the ADM-MO-Jaya algorithm is the most uniform and

converges to a curve in the solution space without isolated points. This may be because the ADM-MO-Jaya algorithm increased the population diversity by randomly adding some populations in the first stage, which in turn improved the convergence of the algorithm. Furthermore, it reduced the iteration step in the later stage, avoiding repeated changes in some positions due to excessive iteration steps. As shown in

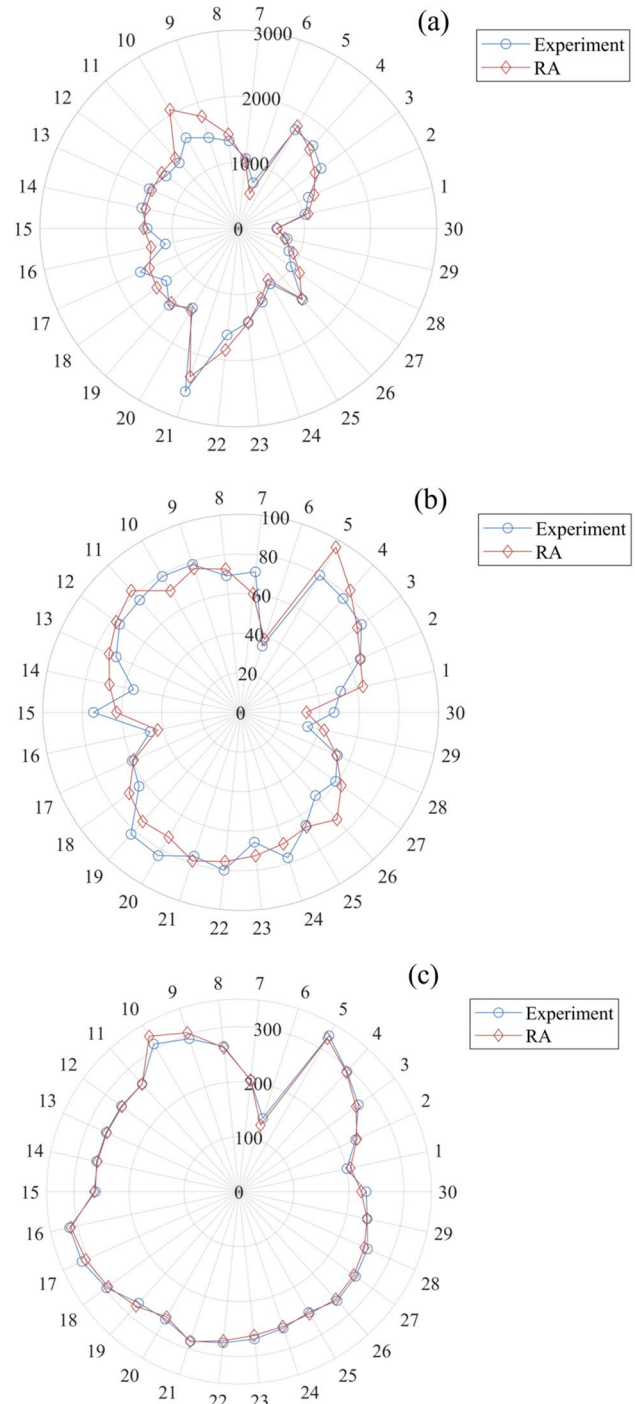
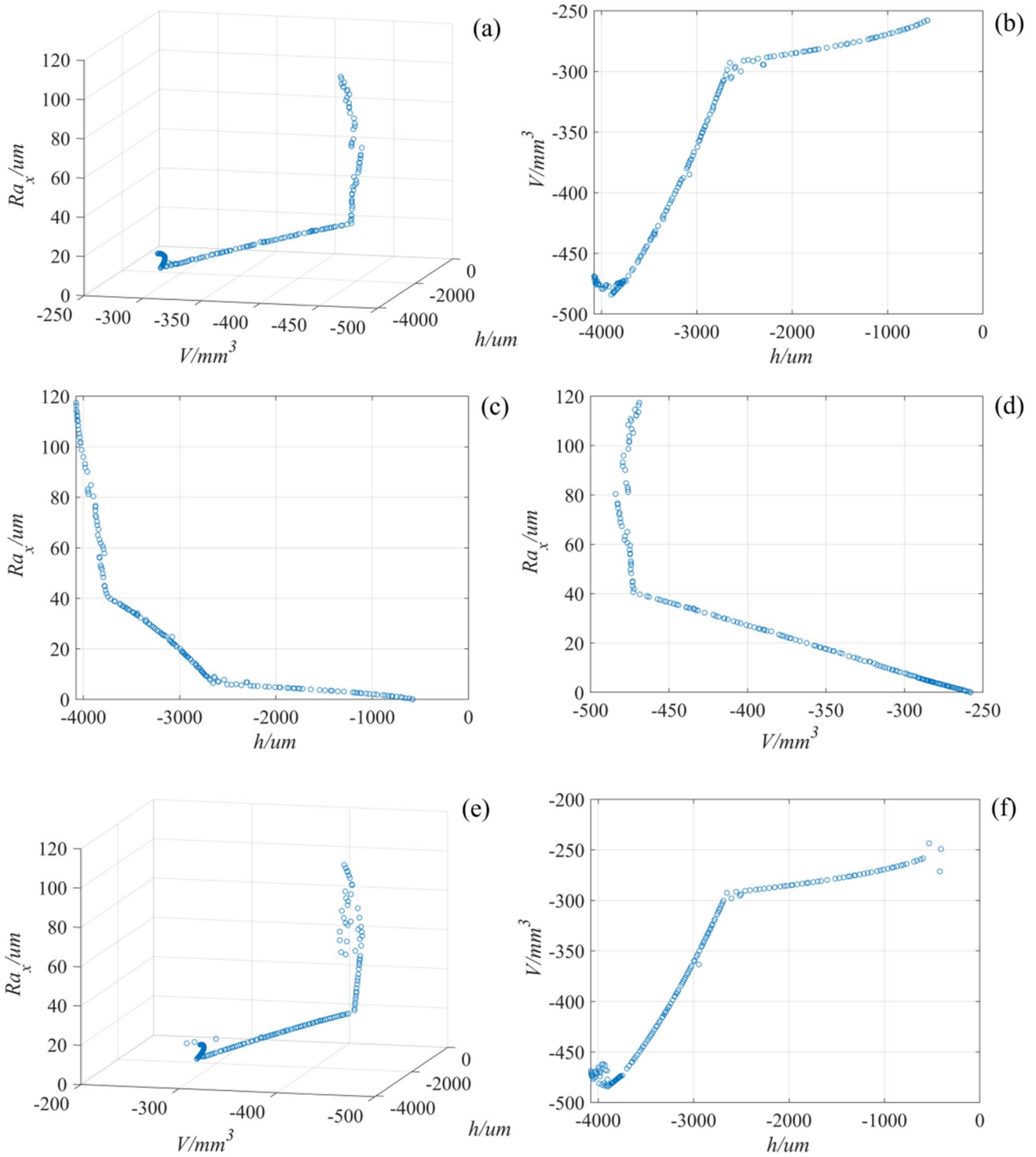


Fig. 10 Predicted and experimental values; a  $h$ , b  $\dot{V}$ , and c  $Ra_x$



**Fig. 11** The Pareto front of three optimization algorithms; **a–d** NSGA-II, **e–h** MO-Jaya, and **i–l** ADM-MO-Jaya algorithm (a), (e), and (i)  $h$ ,  $\dot{V}$ , and  $Ra_x$  Pareto front, the others are two-dimensional diagrams of the three-objective Pareto front

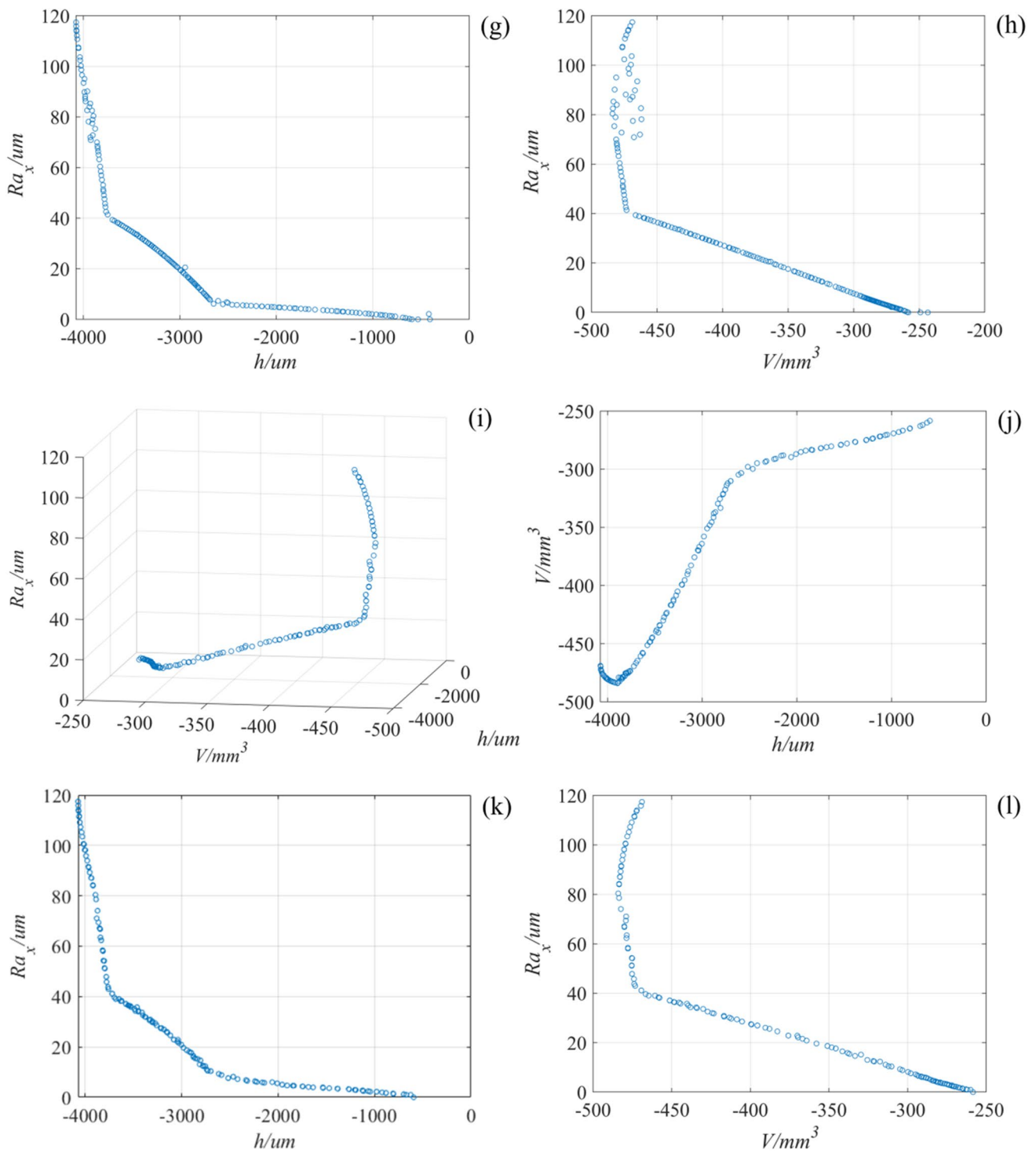


Fig. 11 (continued)

**Table 7** Running time of algorithm; unit: second

| Algorithm   | Mean   | Std   |
|-------------|--------|-------|
| NSGA-II     | 27.419 | 0.215 |
| MO-Jaya     | 92.119 | 1.210 |
| ADM-MO-Jaya | 62.639 | 0.725 |

Table 7, the running time of the three algorithms is approximately 1:2:3. The classical NSGA-II algorithm has the highest operating efficiency, while the MO-Jaya algorithm has the lowest. The operating efficiency of the ADM-MO-Jaya algorithm is 32% higher than that of the MO-Jaya algorithm.

Table 8 shows the 18 solutions extracted from the 180 Pareto fronts optimized by the ADM-MO-Jaya algorithm. In the practical application of AWJ milling of titanium alloys, there is no need to carry out complex process comparisons for operators. They can directly select optimal milling parameters by looking up the Pareto front graph and Table 8 according to the target  $h$ ,  $\dot{V}$ , and  $Ra_x$ . For example, if  $Ra_x < 10 \mu\text{m}$  is the target value, the maximum  $h$  and  $\dot{V}$  could be 2660.999  $\mu\text{m}$  and 303.124  $\text{mm}^3/\text{s}$ , respectively, at  $P = 223.774 \text{ MPa}$ ,  $a = 760.000 \text{ g/min}$ ,  $D = 21.629 \text{ mm}$ ,  $\alpha = 30.065^\circ$ ,  $u = 30.454 \text{ mm/s}$ , and  $S = 0.402 \text{ mm}$ . The results could greatly reduce the dependence on the operator’s machining experience for achieving a high milling quality of AWJ.

**Table 8** Pareto front data of ADM-MO-Jaya algorithm

| Std | $P$ (MPa) | $a$ (g/min) | $D$ (mm) | $\alpha$ ( $^\circ$ ) | $u$ (mm/s) | $S$ (mm) | $h$ ( $\mu\text{m}$ ) | ( $\text{mm}^3/\text{s}$ ) | $Ra_x$ ( $\mu\text{m}$ ) |
|-----|-----------|-------------|----------|-----------------------|------------|----------|-----------------------|----------------------------|--------------------------|
| 1   | 278.975   | 760.000     | 21.857   | 30.037                | 30.000     | 0.401    | 3463.995              | 436.176                    | 34.300                   |
| 2   | 237.946   | 760.000     | 21.724   | 30.000                | 30.283     | 0.400    | 2881.228              | 342.363                    | 16.495                   |
| 3   | 223.774   | 760.000     | 21.629   | 30.065                | 30.454     | 0.402    | 2660.999              | 303.124                    | 9.633                    |
| 4   | 254.865   | 760.000     | 21.374   | 30.253                | 30.063     | 0.400    | 3136.331              | 385.289                    | 25.316                   |
| 5   | 295.726   | 760.000     | 21.573   | 30.292                | 30.250     | 0.400    | 3685.473              | 465.999                    | 40.873                   |
| 6   | 300.000   | 760.000     | 18.721   | 30.854                | 30.031     | 0.400    | 3791.182              | 475.205                    | 50.057                   |
| 7   | 238.909   | 760.000     | 21.553   | 30.606                | 30.255     | 0.400    | 2901.241              | 344.856                    | 18.030                   |
| 8   | 300.000   | 760.000     | 6.000    | 36.255                | 30.062     | 0.400    | 3949.966              | 482.377                    | 89.428                   |
| 9   | 291.864   | 760.000     | 21.697   | 30.000                | 30.006     | 0.400    | 3646.405              | 460.044                    | 38.830                   |
| 10  | 280.001   | 760.000     | 21.512   | 30.049                | 30.000     | 0.400    | 3485.611              | 438.797                    | 35.109                   |
| 11  | 300.000   | 760.000     | 8.954    | 30.013                | 30.000     | 0.400    | 3870.409              | 482.020                    | 73.061                   |
| 12  | 300.000   | 760.000     | 17.052   | 32.544                | 30.000     | 0.400    | 3825.898              | 476.054                    | 56.658                   |
| 13  | 300.000   | 760.000     | 11.764   | 30.893                | 30.000     | 0.400    | 3855.200              | 479.960                    | 67.392                   |
| 14  | 300.000   | 760.000     | 16.860   | 33.821                | 30.093     | 0.400    | 3832.208              | 475.647                    | 59.023                   |
| 15  | 246.089   | 760.000     | 21.781   | 30.018                | 30.140     | 0.400    | 3003.525              | 363.273                    | 20.447                   |
| 16  | 220.018   | 760.000     | 21.970   | 30.000                | 46.823     | 0.400    | 1647.913              | 280.526                    | 4.068                    |
| 17  | 300.000   | 596.611     | 19.333   | 88.674                | 69.956     | 0.799    | 557.543               | 321.210                    | 13.636                   |
| 18  | 220.011   | 760.000     | 21.943   | 30.000                | 67.564     | 0.400    | 792.064               | 264.525                    | 1.426                    |

### 5 Conclusion

In this study, experiments of AWJ milling titanium alloys were designed by considering the process parameters of  $P$ ,  $\dot{m}_a$ ,  $D$ ,  $\alpha$ ,  $u$ , and  $S$ . The effects of these parameters on  $h$ ,  $\dot{V}$ , and  $Ra_x$  were analyzed by using the response surface method. Regression models of  $h$ ,  $\dot{V}$ , and  $Ra_x$  were developed, and the robustness of the models was assessed by ANOVA. Furthermore, the ADM-MO-Jaya algorithm was proposed and verified for multi-objective optimization of AWJ processing parameters, in order to balance the surface roughness and processing efficiency. The concluding remarks of this research are presented below:

1. The  $u$  is the most significant factor on  $h$ , followed by  $\dot{m}_a$ ,  $S$ ,  $P$ ,  $\alpha$ , and  $D$ . For  $\dot{V}$ , the influence of these variables is similar.  $Ra_x$  is most influenced by  $u$ , followed by  $P$ ,  $\dot{m}_a$ ,  $S$ ,  $\alpha$ , and  $D$ , respectively. Based on the response surface analysis, the interactive effect between variables has a significant influence on  $h$ ,  $\dot{V}$ , and  $Ra_x$ .
2. The correlation coefficients  $R^2$  of the model are all greater than 0.9, and the model term is relatively significant. The model residuals obey normal and random distributions, without abnormal structures or obvious styles, and the non-random errors of the experimental data are insignificant.



3. The predicted values of the  $h$ ,  $\dot{V}$ , and  $Ra_x$  regression models are generally consistent with the overall trend of the experimental values. The mean errors of  $h$ ,  $\dot{V}$ , and  $Ra_x$  are 8.57%, 1.89%, and 10.58%, respectively.
4. The Pareto front optimized by the ADM-MO-Jaya algorithm is the most uniform and converges to a curve in the solution space without isolated points. The operation efficiency is 32% higher than the original MO-Jaya algorithm.
5. The optimized set of 180 Pareto solutions can be directly used for milling titanium alloys by AWJ at a relatively high quality without the complex process comparisons.

**Author contribution** Liang Wan: Conceptualization, methodology, and writing—original. Jiayang Liu: Methodology and validation. Yi'an Qian: Analysis and writing—editing. Xiaosun Wang: Methodology. Shijing Wu: Supervision. Hang Du: Experiment. Deng Li: Project administration and writing—review and editing.

**Funding** This research is financially supported by the National Natural Science Foundation of China (nos. 52175245 and 51805188) and the Natural Science Foundation of Hubei Province (no. 2021CFB462).

**Data availability** All the data sets supporting the results are included in the article.

**Code availability** Not applicable.

## Declarations

**Ethics approval** Not applicable.

**Consent to participate** Not applicable.

**Consent for publication** All authors agree to transfer the copyright of this article to the publisher.

**Conflict of interest** The authors declare no competing interests.

## References

1. Sharma D, Singh IV, Kumar J (2022) A microstructure based elasto-plastic polygonal FEM and CDM approach to evaluate LCF life in titanium alloys. *Int J Mech Sci* 225:107356. <https://doi.org/10.1016/j.ijmecsci.2022.107356>
2. Zhang Z, Zhang Y, Liu DH, Zhang YM, Zhao JQ, Zhang GJ (2022) Bubble behavior and its effect on surface integrity in laser-induced plasma micro-machining silicon wafer. *J Manuf Sci E-t Asme* 144(9):091008. <https://doi.org/10.1115/1.4054416>
3. Yang D, Liu Y, Xie F, Xiao X (2019) Analytical investigation of workpiece internal energy generation in peripheral milling of titanium alloy Ti–6Al–4V. *Int J Mech Sci* 161:105063. <https://doi.org/10.1016/j.ijmecsci.2019.105063>
4. An QL, Dang JQ (2020) Cooling effects of cold mist jet with transient heat transfer on high-speed cutting of titanium alloy. *Int J Pr Eng Man-Gt* 7(2):271–282. <https://doi.org/10.1007/s40684-019-00076-7>
5. Farayibi PK, Murray JW, Huang L, Boud F, Kinnell PK, Clare AT (2014) Erosion resistance of laser clad Ti–6Al–4V/WC composite for waterjet tooling. *J Mater Process Tech* 214(3):710–721. <https://doi.org/10.1016/j.jmatprotec.2013.08.014>
6. Wang J, Nguyen T (2021) Mechanisms and predictive models for the erosion process of super hard and brittle materials by a vibration-assisted slurry jet. *Int J Mech Sci* 211:106794. <https://doi.org/10.1016/j.ijmecsci.2021.106794>
7. Armagan M (2021) Cutting of St37 steel plates in stacked form with abrasive water jet. *Mater Manuf Process* 36(11):1305–1313. <https://doi.org/10.1080/10426914.2021.1906895>
8. Krenicky T, Servatka M, Gaspar S, Mascenik J (2020) Abrasive water jet cutting of hardox steels—quality investigation. *Processes* 8(12):1652. <https://doi.org/10.3390/pr8121652>
9. Xiong J, Wan L, Qian YN, Sun S, Li D, Wu SJ (2022) A new strategy for improving the surface quality of Ti6Al4V machined by abrasive water jet: reverse cutting with variable standoff distances. *Int J Adv Manuf Tech* 120(7–8):5339–5350. <https://doi.org/10.1007/s00170-022-09091-6>
10. Umanath K, Devika D, Begum RS (2021) Experimental investigation of the role of particle size and cutting passes in abrasive waterjet machining process on titanium alloy (Ti–6Al–4V) using Taguchi's method. *Mater Manuf Process* 36(8):936–949. <https://doi.org/10.1080/10426914.2020.1866202>
11. Fuse K, Chaudhari R, Vora J, Patel VK, de Lacalle L (2020) Multi-response optimization of abrasive waterjet machining of Ti6Al4V using integrated approach of utilized heat transfer search algorithm and RSM. *Materials* 14(24):7746. <https://doi.org/10.3390/ma14247746>
12. Torrubia PL, Billingham J, Axinte DA (2016) Stochastic simplified modelling of abrasive waterjet footprints. *P Roy Soc A-Math Phys* 472(2186):20150836. <https://doi.org/10.1098/rspa.2015.0836>
13. Anwar S, Axinte DA, Becker AA (2013) Finite element modelling of abrasive waterjet milled footprints. *J Mater Process Tech* 213(2):180–193. <https://doi.org/10.1016/j.jmatprotec.2012.09.006>
14. Kong MC, Anwar S, Billingham J, Axinte DA (2012) Mathematical modelling of abrasive waterjet footprints for arbitrarily moving jets: part I—single straight paths. *Int J Mach Tool Manu* 53(1):58–68. <https://doi.org/10.1016/j.ijmactools.2011.09.010>
15. Fowler G, Pashby IR, Shipway PH (2009) The effect of particle hardness and shape when abrasive water jet milling titanium alloy Ti6Al4V. *Wear* 266(7–8):613–620. <https://doi.org/10.1016/j.wear.2008.06.013>
16. Anwar S, Axinte DA, Becker AA (2013) Finite element modelling of overlapping abrasive waterjet milled footprints. *Wear* 303(1–2):426–436. <https://doi.org/10.1016/j.wear.2013.03.018>
17. Rabani A, Madariaga J, Bouvier C, Axinte D (2016) An approach for using iterative learning for controlling the jet penetration depth in abrasive waterjet milling. *J Manuf Process* 22:99–107. <https://doi.org/10.1016/j.jmapro.2016.01.014>
18. Ozcan Y, Tunc LT, Kopacka J, Cetin B, Sulitka M (2021) Modelling and simulation of controlled depth abrasive water jet machining (AWJM) for roughing passes of free-form surfaces. *Int J Adv Manuf Tech* 114(11–12):3581–3596. <https://doi.org/10.1007/s00170-021-07131-1>
19. Yusup N, Sarkheyli A, Zain AM, Hashim SZM, Ithnin N (2014) Estimation of optimal machining control parameters using artificial bee colony. *J Intell Manuf* 25(6):1463–1472. <https://doi.org/10.1007/s10845-013-0753-y>
20. Mohamad A, Zain AM, Bazin NEN, Udin A (2015) A process prediction model based on Cuckoo algorithm for abrasive waterjet machining. *J Intell Manuf* 26(6):1247–1252. <https://doi.org/10.1007/s10845-013-0853-8>

21. Chakraborty S, Mitra A (2018) Parametric optimization of abrasive water-jet machining processes using grey wolf optimizer. *Mater Manuf Process* 33(13):1471–1482. <https://doi.org/10.1080/10426914.2018.1453158>
22. Shukla R, Singh D (2017) Experimentation investigation of abrasive water jet machining parameters using Taguchi and evolutionary optimization techniques. *Swarm Evol Comput* 32:167–183. <https://doi.org/10.1016/j.swevo.2016.07.002>
23. Rao RV, Rai DP, Balic J (2019) Multi-objective optimization of abrasive waterjet machining process using Jaya algorithm and PROMETHEE method. *J Intell Manuf* 30(5):2101–2127. <https://doi.org/10.1007/s10845-017-1373-8>
24. Rao RV, Saroj A (2017) A self-adaptive multi-population based Jaya algorithm for engineering optimization. *Swarm Evol Comput* 37:1–26. <https://doi.org/10.1016/j.swevo.2017.04.008>
25. Rao R (2016) Jaya: A simple and new optimization algorithm for solving constrained and unconstrained optimization problems. *Int J Ind Eng Comp* 7:19–34. <https://doi.org/10.5267/j.ijiec.2015.8.004>
26. Bui V, Gilles P, Sultan T, Cohen G, Rubio W (2017) A new cutting depth model with rapid calibration in abrasive water jet machining of titanium alloy. *Int J Adv Manuf Tech* 93(5–8):1499–1512. <https://doi.org/10.1007/s00170-017-0581-x>
27. Hlavac LM, Krajcarz D, Hlavacova IM, Spadlo S (2017) Precision comparison of analytical and statistical-regression models for AWJ cutting. *Precis Eng* 50:148–159. <https://doi.org/10.1016/j.precisioneng.2017.05.002>
28. Deb K, Pratap A, Agarwal S, Meyarivan T (2002) A fast and elitist multiobjective genetic algorithm: NSGA-II. *Ieee T Evolut Comput* 6(2):182–197. <https://doi.org/10.1109/4235.996017>
29. Sourd X, Zitoune R, Crouzeix L, Salem M, Charlas M (2020) New model for the prediction of the machining depth during milling of 3D woven composite using abrasive waterjet process. *Compos Struct* 234:111760. <https://doi.org/10.1016/j.compstruct.2019.111760>
30. Sultan T, Gilles P, Cohen G, Cenac F, Rubio W (2016) Modeling incision profile in AWJM of titanium alloys Ti6Al4V. *Mech Ind* 17(4):403. <https://doi.org/10.1051/meca/2015102>
31. Cenac F, Zitoune R, Collombet F, Deleris M (2015) Abrasive water-jet milling of aeronautic aluminum 2024–T3. *P I Mech Eng L-J Mat* 229(1):29–37. <https://doi.org/10.1177/1464420713499288>

**Publisher's note** Springer Nature remains neutral with regard to jurisdictional claims in published maps and institutional affiliations.

Springer Nature or its licensor (e.g. a society or other partner) holds exclusive rights to this article under a publishing agreement with the author(s) or other rightsholder(s); author self-archiving of the accepted manuscript version of this article is solely governed by the terms of such publishing agreement and applicable law.